

NACA RM L54A20

7518



NACA

# RESEARCH MEMORANDUM

AERODYNAMIC CHARACTERISTICS AT TRANSONIC AND SUPERSONIC  
SPEEDS OF A ROCKET-PROPELLED AIRPLANE CONFIGURATION

HAVING A  $52.5^\circ$  DELTA WING AND A LOW,  
SWEPT HORIZONTAL TAIL

By Alan B. Kehlet

Langley Aeronautical Laboratory  
Langley Field, Va.

NATIONAL ADVISORY COMMITTEE  
FOR AERONAUTICS

WASHINGTON  
March 29, 1954

Classification cancelled (or changed to) UNCLASSIFIED

By Authority of NASA Tech Rep Announcement #124  
(OFFICER AUTHORIZED TO CHANGE)

By 10 FEB 58  
NAME AND

HARR  
GRADE OF OFFICER MAKING CHANGE)

28 Mar 61  
DATE



0144269

NACA RM L54A20

~~CONFIDENTIAL~~

## NATIONAL ADVISORY COMMITTEE FOR AERONAUTICS

## RESEARCH MEMORANDUM

AERODYNAMIC CHARACTERISTICS AT TRANSONIC AND SUPERSONIC  
SPEEDS OF A ROCKET-PROPELLED AIRPLANE CONFIGURATION  
HAVING A  $52.5^\circ$  DELTA WING AND A LOW,  
SWEEP HORIZONTAL TAIL

By Alan B. Kehlet

## SUMMARY

A flight investigation over a Mach number range from 0.79 to 1.83 has been conducted in order to determine the aerodynamic characteristics at low lift of a rocket model of an airplane configuration having a  $52.5^\circ$  delta wing of aspect ratio 3.08 with NACA 65A003 airfoil sections in the streamwise direction and a low, swept horizontal tail. The lift-curve slopes and static longitudinal stability were nonlinear with lift coefficient over most of the Mach number range and increased with increasing lift coefficient over the lift range covered. The minimum drag coefficient increased from 0.016 to 0.035 through the transonic speed range.

The model damping characteristics were irregular and altered for the two tail settings over the Mach number range covered with the higher-lift tail setting having the greater damping.

The measured periods of the lateral oscillations were of the same order of magnitude as the longitudinal periods, but apparently were not affected by lift coefficient. The model exhibited stable static directional characteristics throughout the Mach number range tested.

## INTRODUCTION

As part of a general research program investigating longitudinal stability of wings having various plan forms and thickness ratios, a rocket-propelled model of an airplane configuration having a  $52.5^\circ$  delta wing of aspect ratio 3.08 has been flown. The basic fuselage-empennage configuration (ref. 1) had swept horizontal and vertical tails with the

~~CONFIDENTIAL~~*Handwritten signature*

all-movable horizontal tail mounted in a low position. During the flight, the horizontal tail was deflected in a square-wave program between  $0.10^\circ$  and  $-3.2^\circ$ .

The model was flown at the Langley Pilotless Aircraft Research Station at Wallops Island, Va.

#### SYMBOLS

$C_N$	normal-force coefficient, $\frac{a_n}{g} \frac{W/S}{q}$
$C_C$	chord-force coefficient, $-\frac{a_l}{g} \frac{W/S}{q}$
$C_L$	lift coefficient, $C_N \cos \alpha - C_C \sin \alpha$
$C_D$	drag coefficient, $C_C \cos \alpha + C_N \sin \alpha$
$C_{L0}$	lift coefficient at minimum drag coefficient
$C_m$	pitching-moment coefficient about center of gravity
$a_n$	normal acceleration determined from accelerometer, ft/sec <sup>2</sup>
$a_l$	longitudinal acceleration determined from accelerometer, ft/sec <sup>2</sup>
$g$	acceleration of gravity, ft/sec <sup>2</sup>
$q$	dynamic pressure, $0.70pM^2$
$p$	free-stream static pressure, lb/sq ft
$M$	Mach number
$R$	Reynolds number, based on wing mean aerodynamic chord
$S$	wing area (including area enclosed by fuselage), sq ft
$\bar{c}$	wing mean aerodynamic chord (M.A.C.), ft
$b$	wing span, ft
$W$	weight, lb

A	cross-sectional area, sq in.
r	equivalent radius of cross-sectional area, in. $\sqrt{A/\pi}$
X	longitudinal distance from station 0, in.
l	length of model, in.
P	period of oscillation, sec
$T_{1/2}$	time to damp to one-half amplitude, sec
$\alpha$	angle of attack, deg
$\delta$	control panel deflection (measured free stream normal to wing chord plane), deg
$\theta$	angle of pitch, radians
$\beta$	angle of sideslip, deg

$$C_{m_q} = \frac{dC_m}{d\left(\frac{q\bar{c}}{2V}\right)}$$

$$C_{m_{\dot{\alpha}}} = \frac{dC_m}{d\left(\frac{\dot{\alpha}\bar{c}}{2V}\right)}$$

$C_{n_{\beta}^*}$  effective rate of change of yawing-moment coefficient with sideslip angle per degree (derived as in ref. 7)

$$\frac{dC_D}{dC_L^2} = \frac{dC_D}{d(C_L - C_{L0})^2}$$

Subscripts:

w	wing
f	fuselage

$$\dot{\alpha} = \frac{1}{57.3} \frac{d\alpha}{dt}$$

$$q = \frac{d\theta}{dt}$$

The symbols  $\alpha$ ,  $\dot{\alpha}$ ,  $q$ ,  $\delta$ , and  $\beta^*$  used as subscripts indicate the derivative of the quantity with respect to the subscript; for

example,  $C_{L_\alpha} = \frac{dC_L}{d\alpha}$ .

### MODEL AND INSTRUMENTATION

#### Model

A three-view drawing of the model is shown in figure 1. The non-dimensional equivalent body and area distribution, presented for possible drag correlation purposes, are shown in figure 2. Photographs of the model are shown in figure 3.

The empennage has a vertical fin of wood and aluminum with the quarter-chord line swept  $60^\circ$  and NACA 65A003 airfoil sections in the streamwise direction; a horizontal tail of duralumin with the quarter-chord line swept  $45^\circ$  with  $20^\circ$  negative dihedral and NACA 65A006 airfoil sections in the streamwise direction perpendicular to the chord plane. The fuselage is described in reference 2.

The steel delta wing of aspect ratio 3.08 had a leading-edge sweep of  $52.5^\circ$  and NACA 65A003 airfoil sections in the streamwise direction.

Each panel of the horizontal tail was deflected in an approximate square-wave program by a separate servo-control fed by a common pressure system and regulated by an electric motor-driven selector valve. For the present investigation, the stop positions were  $0.1^\circ$  and  $-3.2^\circ$  measured parallel to the model center line and normal to the wing chord plane.

The model weighed 118.75 pounds and had a moment of inertia in pitch and yaw of 8.21 and 8.31 slug-ft<sup>2</sup>, respectively. The center of gravity was located at 0.26 of the wing mean aerodynamic chord.

## Instrumentation

The model was equipped with an NACA telemetering system which transmitted continuous measurements of normal acceleration at the center of gravity, normal acceleration at a reference nose station, angle of attack, longitudinal acceleration, transverse acceleration, control position, total pressure, and reference static pressure.

Flight-path information was obtained from tracking radar and atmospheric conditions at altitude from a radiosonde released immediately after the flight. Motion-picture cameras were used to photograph the launching and first portion of the flight.

## TESTS AND DATA REDUCTION

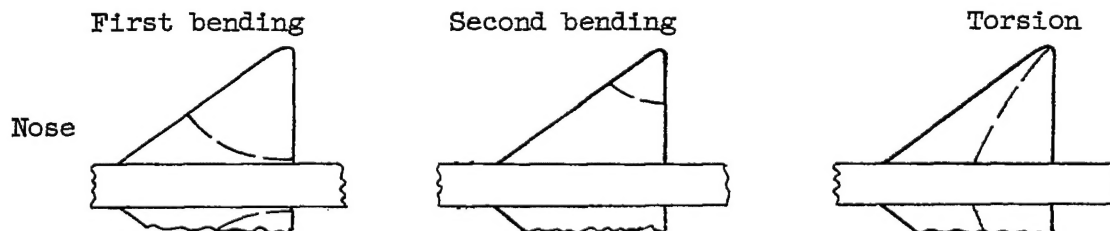
### Preflight Tests

Prior to instrumentation, the model was placed in a profile machine and measurements were made in the streamwise direction of the airfoil sections, perpendicular to the chord planes of the vertical and horizontal tails and of the wing. These measurements were used to check construction tolerances.

Prior to flight testing and with the instruments installed, the model was suspended by shock chords and vibrated by an electromagnetic shaker. The following model natural frequencies and modes of vibration were determined:

	First bending, cps	Second bending, cps	Torsion, cps
Horizontal tail . . .	100		
Vertical tail . . . .	57		
Wing . . . . .	116	164	370

### Wing Modes



### Flight Tests

The model was launched at an angle of approximately  $60^\circ$  from the horizontal by means of a mobile launcher as shown in figure 3. Two 6-inch-diameter solid-fuel ABL Deacon rocket motors boosted the model to maximum velocity. All measurements used were taken during the decelerating portion of the flight.

### Data Reduction

The response of the model to deflections of an all-movable horizontal tail in an approximate square-wave program was analyzed by the method of reference 3. The indicated angles of attack were corrected to angles of attack at the model center of gravity by the method of reference 4. The two-accelerometer method for obtaining instantaneous total pitching-moment coefficients was used as described in reference 2.

### ACCURACY

The absolute accuracy of the measured quantities is impossible to establish because the instrument calibrations can not be checked during or after the flight. Most of the probable instrumentation errors occur as errors in absolute magnitude. Incremental values or slopes should, in general, be more accurate than the absolute values. An indication of the systematic instrument errors possible is given by the following table, based on an accuracy of  $\pm 1$  percent of the full instrument range:

M	$C_N$	$C_C$
1.7	$\pm 0.00490$	$\pm 0.00122$
1.0	$\pm 0.02251$	$\pm 0.00563$
.8	$\pm 0.04180$	$\pm 0.01045$

The CW Doppler radar unit is believed to be accurate to better than 1 percent for nonmaneuvering models. The Mach number at peak velocity should, therefore, be accurate to 1 percent or better. Since the Mach number subsequent to peak velocity was determined from telemetric data, it probably becomes less accurate as the Mach number decreases.

Further errors in the aerodynamic coefficients may arise from possible dynamic-pressure inaccuracies which are approximately twice as great as errors in Mach number.



An indication of random errors encountered may be noted from the scatter of data points shown in the figures. Errors in angle of attack and control panel deflection are independent of dynamic pressure and are not likely to vary with Mach number. The horizontal-tail deflections are estimated to be accurate within  $\pm 0.10^\circ$  and the increments in angle of attack within  $\pm 0.20^\circ$ .

## RESULTS AND DISCUSSION

Dynamic pressure and Reynolds number obtained during the flight are shown in figures 4 and 5, respectively. A typical time history at the higher Mach numbers of some of the quantities measured is shown in figure 6. Hereafter, in order to distinguish the two tail settings, the deflection of  $0.1^\circ$  shall be referred to as the low-lift tail setting and the deflection of  $-3.2^\circ$  as the higher-lift tail setting.

### Longitudinal Trim

The variations of the trim lift coefficient and trim angle of attack at the two control settings as functions of Mach number are shown in figure 7. At transonic speeds and with increasing Mach number, the model exhibited a trim change of approximately  $1^\circ$  nose-up in the low lift range; whereas at the higher trimmed lift condition, a nose-down trim change of approximately  $2^\circ$  occurred.

### Lift

The variation of the lift coefficient with angle of attack over the Mach number range is shown in figure 8. The lift-curve slopes represented by the faired lines in figure 8 are presented as functions of Mach number in figure 9 for both tail settings. Included in figure 9 for comparative purposes are the lift-curve-slope data for a wind-tunnel model with a similar wing-fuselage combination having no horizontal tail (ref. 5). In view of the differences in models, the agreement between the rocket-model data and the wind-tunnel data is considered good. It is indicated in figure 9 that the lift coefficient does not vary linearly with the angle of attack, particularly at the lower Mach numbers; however, reference to the trim lift coefficients (fig. 7), which are indicative of the lift ranges covered by the two tail settings, shows that the linearity of the lift-curve slopes present at the higher Mach numbers may be due to the low lift range of the higher-lift tail setting and not entirely to a Mach number effect. The increase in lift-curve slope with increasing lift coefficient, where nonlinearity occurs, is believed to be due in part to a decrease in the downwash field over the low horizontal tail with increasing angle of attack of the model and to a nonlinearity in the lift-curve slope of the long nose section of the fuselage.

### Drag

The variation of drag coefficient with lift coefficient corresponding to the lift ranges of figure 8 is shown in figure 10. The maximum lift-drag ratios that could be measured from figure 10 and lift coefficient at which  $(L/D)_{\max}$  occurs are shown in figure 11. Because of the reduced amplitude of the oscillations, the model never reached its maximum lift-drag ratios at Mach numbers greater than 1.12; values of  $(L/D)_{\max}$  and  $C_L$  for  $(L/D)_{\max}$  obtained at higher Mach numbers were extrapolated from the data for the drag due to lift, minimum drag coefficient, and lift coefficient at minimum drag. At high subsonic speeds, the maximum value of the maximum lift-drag ratios obtained was about 9, decreasing to about 6 at low supersonic speeds and to about  $4\frac{1}{2}$  at the test's limit; the values of lift coefficient corresponding to these values are about 0.25, 0.40, and 0.30, respectively.

The minimum drag coefficient and the lift coefficient at minimum drag coefficient obtained from figure 10 are presented as a function of Mach number in figure 12. The flagged symbols on the minimum-drag-coefficient curve indicate extrapolated points from the higher-lift tail setting. It should be noted that, as indicated by the basic data of figure 10, the values of the minimum drag coefficient correspond closely to the values of the zero lift-drag coefficient, the drag polars at the low-lift tail setting are flat around zero lift coefficient, and the values of the lift coefficient at minimum drag can be determined, with any degree of accuracy, only below a Mach number of 1.3. At all Mach numbers for the higher-lift tail setting, no lift coefficient at minimum drag can be obtained.

By using the values of the lift coefficient at minimum drag coefficient (fig. 12) for the low-lift tail setting and by interpolating values for the higher-lift tail setting, the effect of lift on drag as a function of Mach number was determined and is presented in figure 13. As indicated by the data of figure 13, the model exhibited poor leading-edge suction over the Mach number range where the effect of lift on drag could be determined. As stated before, prior to instrumentation, measurements of the airfoil sections were made. The wing airfoil sections, as determined from these measurements, revealed a leading-edge radius somewhat smaller than the true NACA 65A003 airfoil section. The resulting rather sharp leading edge is believed to be part of the cause of the lack of leading-edge suction obtained.

### Longitudinal Static Stability

The measured periods of the longitudinal oscillations for both tail settings as a function of Mach number and the longitudinal-static-stability parameter  $C_{m\alpha}$  determined from these periods are presented in

figures 14 and 15, respectively. As with the lift-curve slopes (fig. 9), the nonlinearity present in the data decreased with increasing Mach number. Where nonlinearity of the data occurred, the higher-lift tail setting had the greater value of static stability. Again, however, the linearity at the higher Mach numbers may be due to the decreasing trim lift coefficient rather than to the increasing Mach number.

The variation of the static-stability parameter is reflected in the aerodynamic-center location for the two tail settings (fig. 16). The data at both tail settings exhibited a rearward movement of the aerodynamic center up to a Mach number of about 1.5 with the higher-lift tail setting having the greater stability. Above  $M = 1.5$ , a forward movement occurs.

The variation of the total pitching-moment coefficient, obtained from the two-accelerometer method (ref. 2), with lift coefficient is shown in figure 17. Although some scatter is present, particularly at subsonic speeds, the data agree, in general, with the slopes indicated by the period method and the trim data of figure 7 which are also shown in figure 17.

A measure of the horizontal-tail effectiveness in producing moment and ability to produce lift, as obtained from an average of  $C_{m\alpha}$  for the two tail settings (fig. 15), the trim angle of attack (fig. 7), and an estimated tail length, is presented in figure 18. Both parameters exhibit the same general shape as the lift-curve slopes (fig. 9), that is, increasing with Mach number to  $M = 1.0$  and then decreasing with increasing Mach number. At the test limit ( $M \approx 1.83$ ), a decrease of approximately 50 percent of that at  $M = 1.0$  is noted in both parameters. Included in figure 18 for comparative purposes are  $CL_6$  and  $CL_8$ , obtained from  $CL_\alpha$  from the exposed duralumin wing of reference 2 (extrapolated  $CL_\alpha$  at the higher Mach numbers) and corrected for dihedral effects.

Although the values obtained from reference 2 are approximately 20 percent higher throughout the Mach number range covered, it should be pointed out that the duralumin wing  $CL_\alpha$  used was not corrected for the small gap that exists between the fuselage and horizontal-tail panel. The effects of a small gap in a nonviscous flow (ref. 6) can be large, reducing the lift-curve slope by as much as 40 percent. By using an average gap of 0.076 inch and  $CL_\alpha$  from reference 2, an estimate of the effect of the gap at  $M = 1.00$  was made. The gap reduced the parameters by about 30 percent (about 15 percent lower than the model values). However, since the flow is viscous and, therefore, the effective gap is smaller than the measured gap, the tail parameters obtained from  $CL_\alpha$  of reference 2 and corrected for an effective gap should, in general, be close to the values obtained from the model.

### Damping in Pitch

The variations of the amplitude ratio (the ratio of the amplitude from the trim line of successive oscillations to the initial oscillation) with time, for both tail settings, are shown in figure 19. The time to damp to one-half amplitude, represented by the time required for the faired line to cross 0.50 amplitude ratio (fig. 19), as a function of Mach number, and the pitch damping-moment factors are shown in figure 20. As with the lift-curve slope and period data, nonlinearity with the trim lift coefficient was also present in the time to damp to one-half amplitude over all but the higher Mach numbers. Where nonlinearity occurred, the model exhibited irregular damping characteristics with the higher-lift tail setting having the greater damping. Since, for the configuration used in this investigation, damping is primarily due to the tail and would be expected to decrease as downwash over the tail decreases, and, since, in the discussion of lift, downwash was believed to decrease over the tail with increasing angle of attack, the model damping at the higher-lift tail setting would be expected to be less than the damping at the low-lift tail setting. The reasons for the altered damping characteristics are not known at this time; however, since the model exhibited both longitudinal and lateral oscillations, the possibility exists of coupling between these oscillations. The effect of coupling is believed to tend to reduce the model damping.

### Directional Static Stability

Although the primary purpose of the model flown in this investigation was longitudinal stability, lateral oscillations were present and, therefore, were investigated. These oscillations are believed to be caused by some asymmetry in the horizontal-tail stops that could be present and cause lateral disturbances.

The variation of the measured periods of the lateral oscillations as a function of Mach number and the static-directional-stability coefficient (derived as in ref. 7) as determined from these periods are presented in figures 21 and 22, respectively. Throughout the Mach number range the measured periods of the lateral oscillation are of the same order of magnitude as the measured periods of the longitudinal oscillations and appear to be unaffected by lift coefficient over the lift range covered. Although some coupling between the longitudinal and lateral oscillations is probably present, the effect of this coupling is believed to be small on all the aerodynamic parameters with the exception of the damping in pitch.

The static-directional-stability coefficient exhibited a decrease of about 30 percent from the high subsonic to the highest supersonic Mach numbers. Flexibility becomes increasingly important with increasing

Mach number, and the decrease in the static-directional-stability coefficient is believed to be due in part to flexibility of the vertical tail. Reference to the table of natural frequencies indicates that the vertical tail is rather flexible. At the Mach numbers covered, however, the model exhibited stable static directional characteristics.

An estimation of the approximate maximum amplitudes of the angle of sideslip over the Mach number range covered has been made. At the high subsonic Mach numbers, maximum amplitudes of  $\pm 2^\circ$  and  $\pm 3^\circ$  occurred for the higher- and low-lift tail settings, respectively; these amplitudes decreased to about half at the transonic and supersonic Mach numbers.

### CONCLUSIONS

A flight investigation of the aerodynamic characteristics at transonic and supersonic speeds of a rocket-propelled airplane configuration having a  $52.5^\circ$  delta wing and a low, swept horizontal tail indicated the following conclusions:

1. At transonic speeds and with increasing Mach number, the model exhibited a trim change of approximately  $1^\circ$  nose-up in the low lift range and a  $2^\circ$  nose-down trim change while trimmed at the higher lift condition.
2. The lift-curve slopes were nonlinear in the transonic and low supersonic Mach number range and increased with lift coefficient over the lift range covered.
3. The minimum drag coefficient increased from 0.016 to 0.035 through the transonic speed range. The minimum drag coefficient was close to the drag coefficient at zero lift.
4. Over the Mach number range where it could be determined, the model exhibited poor leading-edge suction.
5. The aerodynamic center moved rearward with increasing Mach number up to a Mach number of about 1.5, with greater stability at the higher lifts.
6. The model damping characteristics were irregular and altered for the two tail settings over the Mach number range covered with the higher-lift tail setting having the greater damping.

7. The model exhibited stable static directional characteristics over the Mach number and lift ranges covered.

Langley Aeronautical Laboratory,  
National Advisory Committee for Aeronautics,  
Langley Field, Va., January 7, 1954.

#### REFERENCES

1. McFall, John C., Jr.: Longitudinal Stability Characteristics at Transonic Speeds of a Rocket-Propelled Model of an Airplane Configuration Having a  $45^\circ$  Swept Wing of Aspect Ratio 6.0. NACA RM L53G22a, 1954.
2. Vitale, A. James: Effects of Wing Elasticity on the Aerodynamic Characteristics of an Airplane Configuration Having  $45^\circ$  Sweptback Wings As Obtained From Free-Flight Rocket-Model Tests at Transonic Speeds. NACA RM L52L30, 1953.
3. Gillis, Clarence L., Peck, Robert F., and Vitale, A. James: Preliminary Results From a Free-Flight Investigation at Transonic and Supersonic Speeds of the Longitudinal Stability and Control Characteristics of an Airplane Configuration With a Thin Straight Wing of Aspect Ratio 3. NACA RM L9K25a, 1950.
4. Mitchell, Jesse L., and Peck, Robert F.: An NACA Vane-Type Angle-of-Attack Indicator for Use at Subsonic and Supersonic Speeds. NACA RM L9F28a, 1949.
5. Heitmeyer, John C.: Effect of Vertical Position of the Wing on the Aerodynamic Characteristics of Three Wing-Body Combinations. NACA RM A52L15a, 1953.
6. Bleviss, Z. O., and Struble, R. A.: Some Effects of Streamwise Gaps on the Aerodynamic Characteristics of Low-Aspect-Ratio Lifting Surfaces at Supersonic Speeds. Rep. No. SM-14627, Douglas Aircraft Co., Inc., Apr. 1, 1953.
7. Purser, Paul E., and Mitchell, Jesse L.: Miscellaneous Directional-Stability Data for Several Airplane-Like Configurations From Rocket-Model Tests at Transonic Speeds. NACA RM L52E06b, 1952.

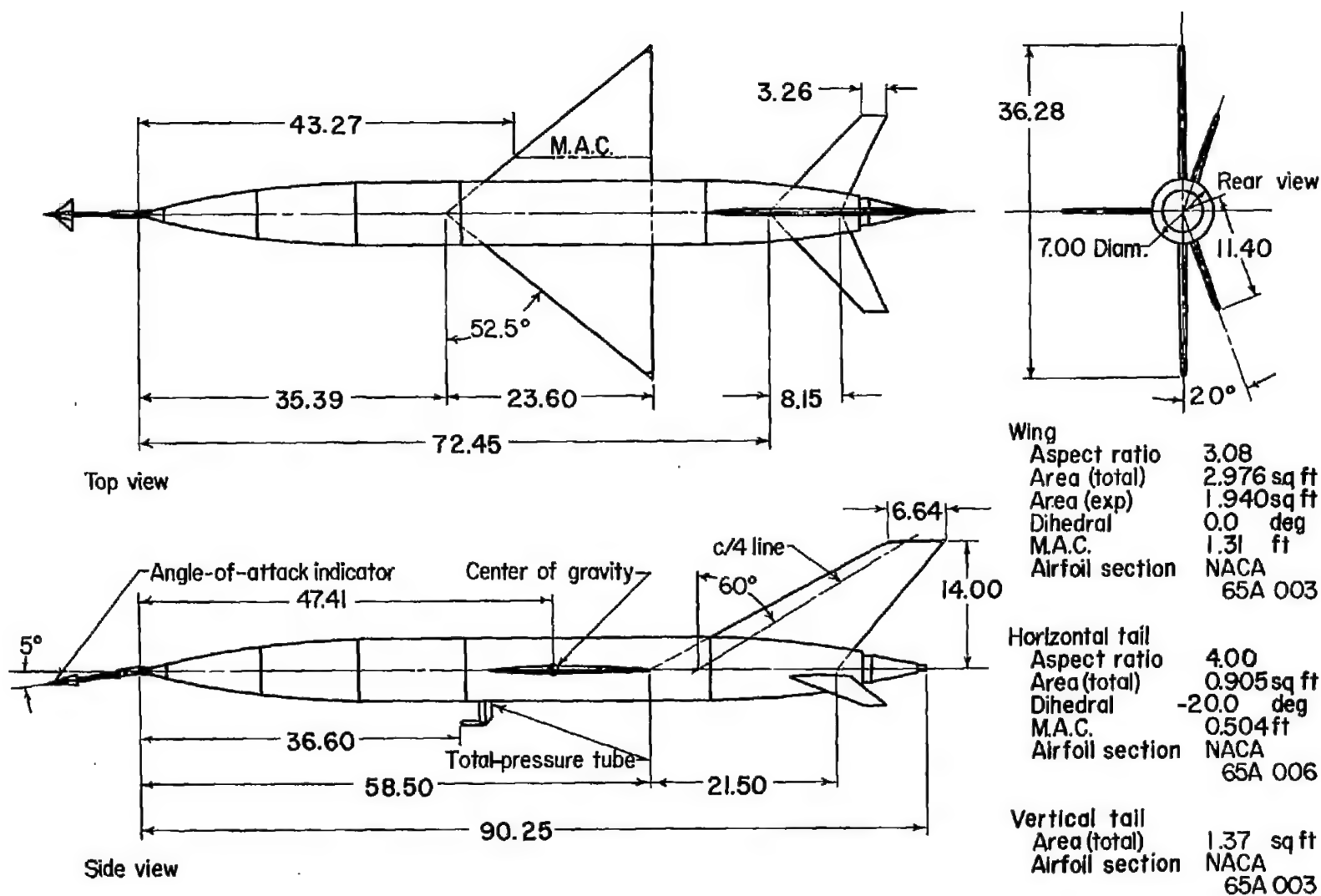
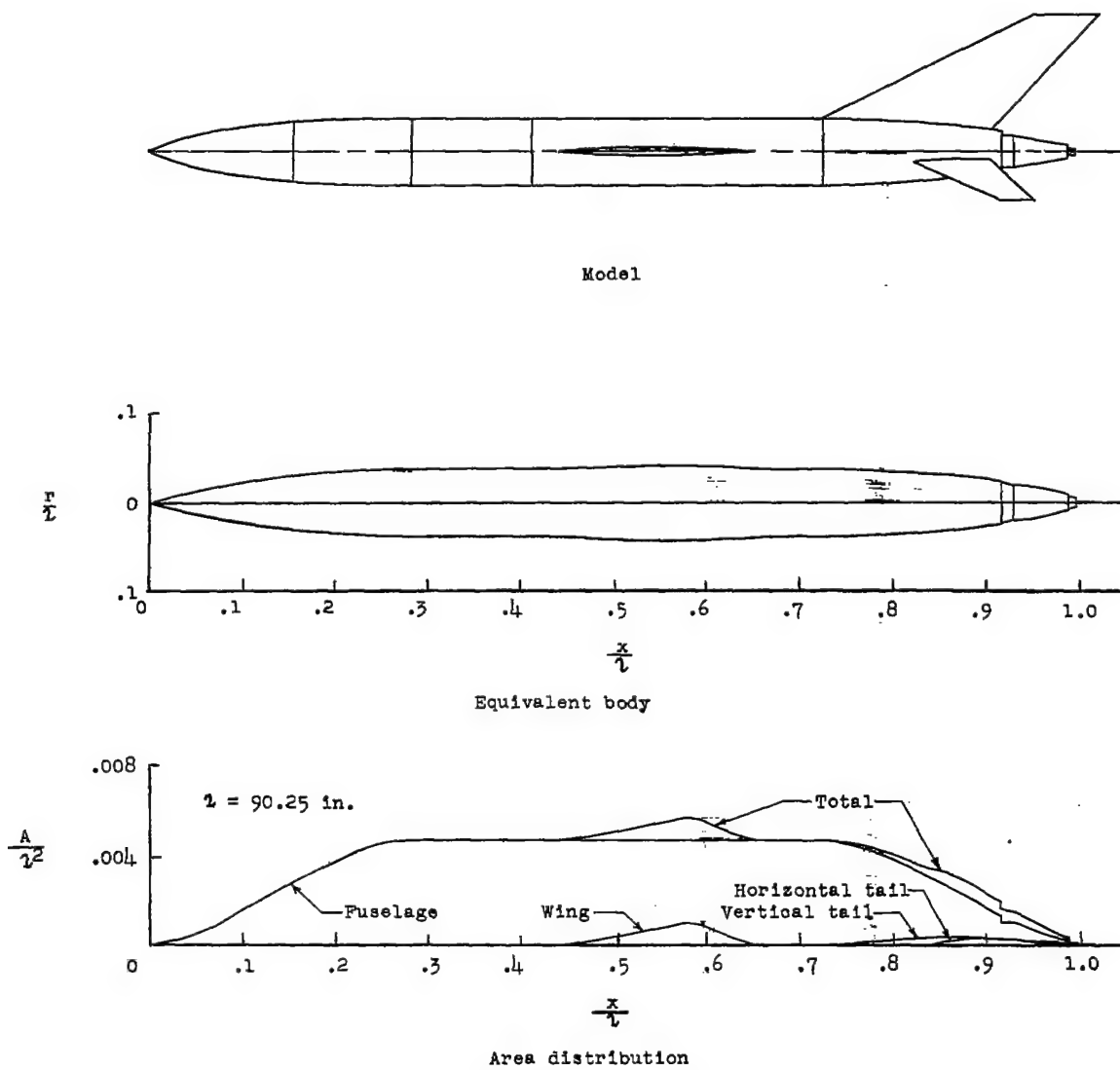
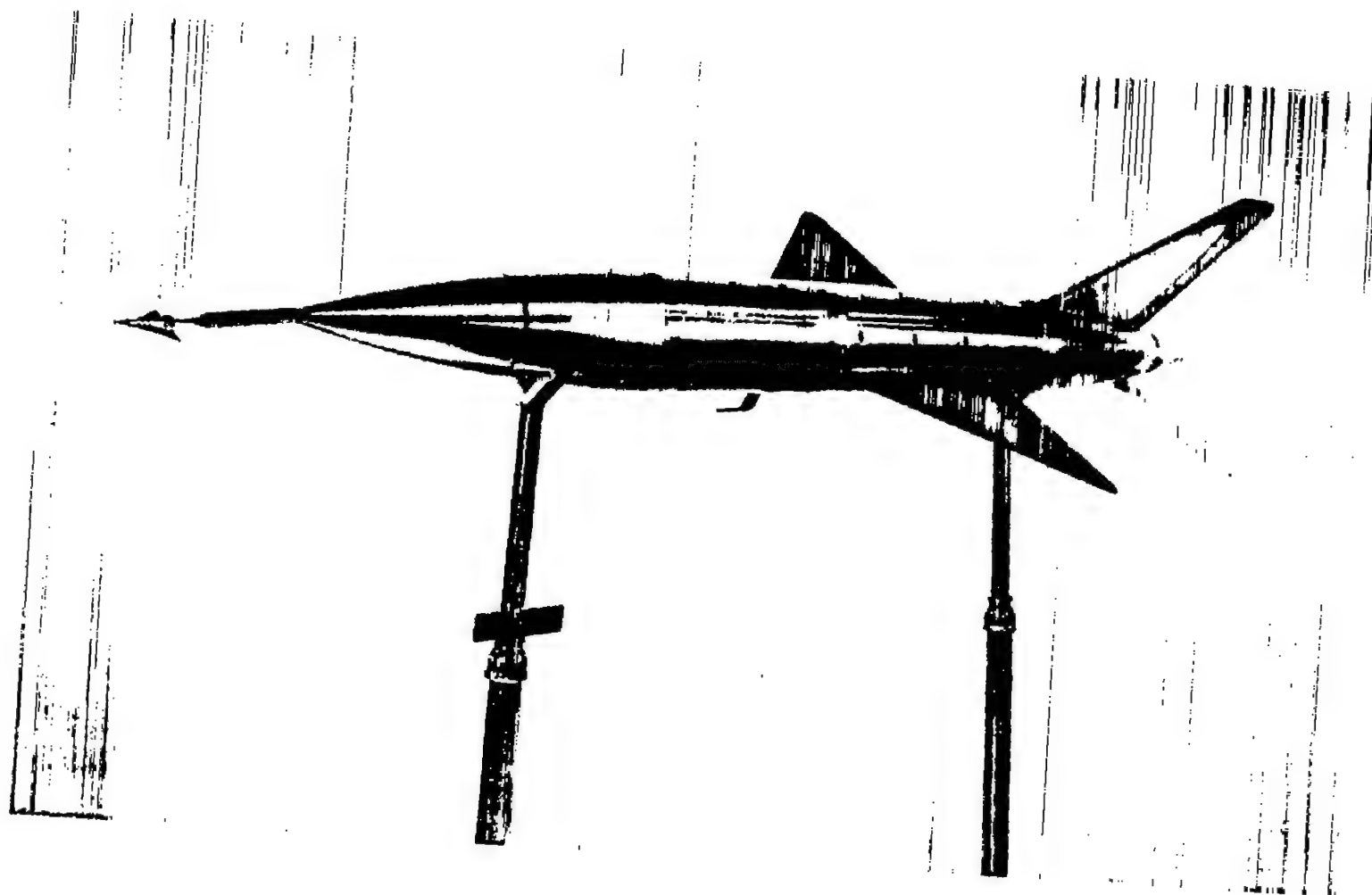


Figure 1.- General arrangement of model. All dimensions are in inches.

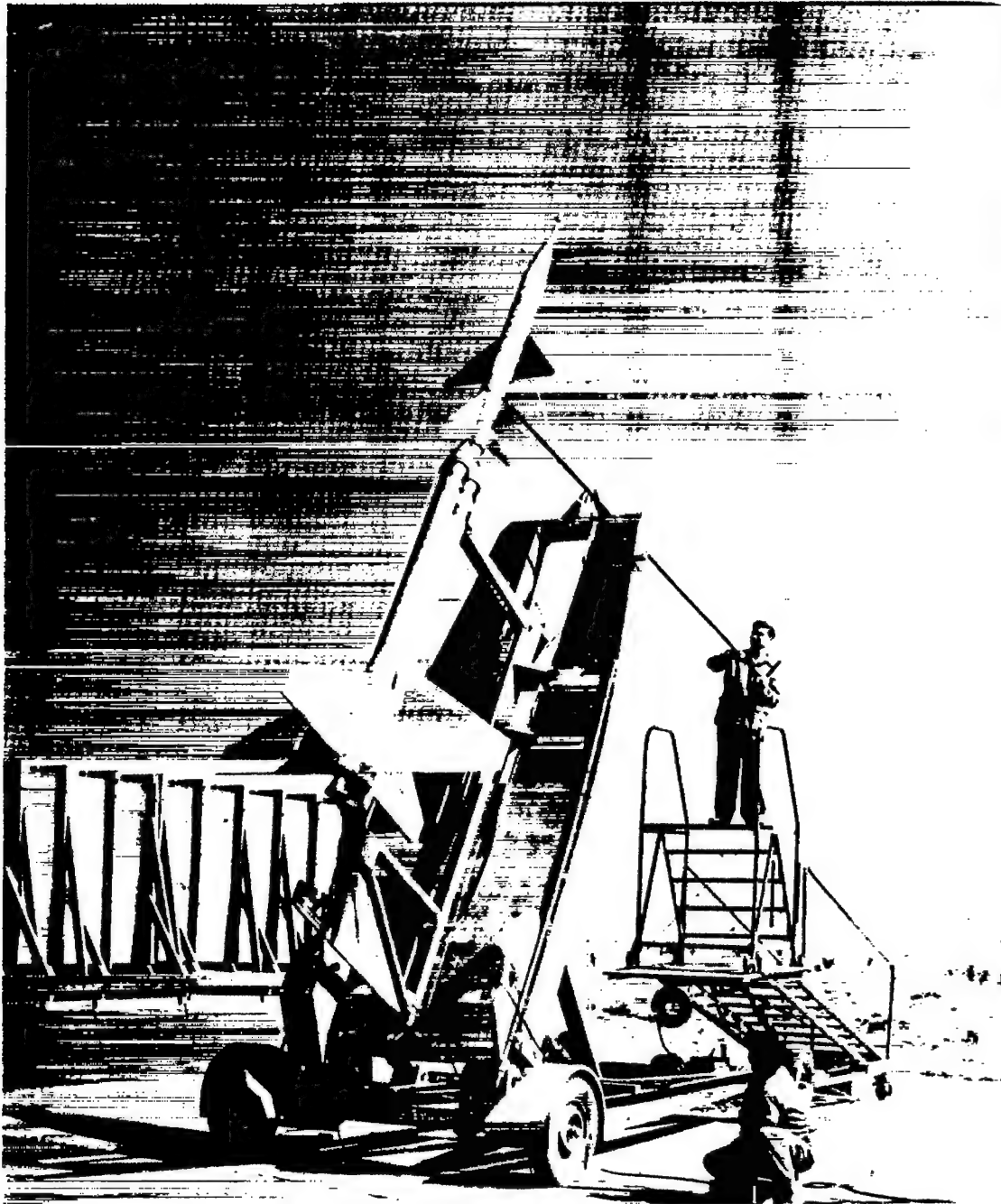






(a) Three-quarter front view. L-79378.1

Figure 3.- Photographs of models.



L-79541

(b) Model on launcher.

Figure 3.- Concluded.

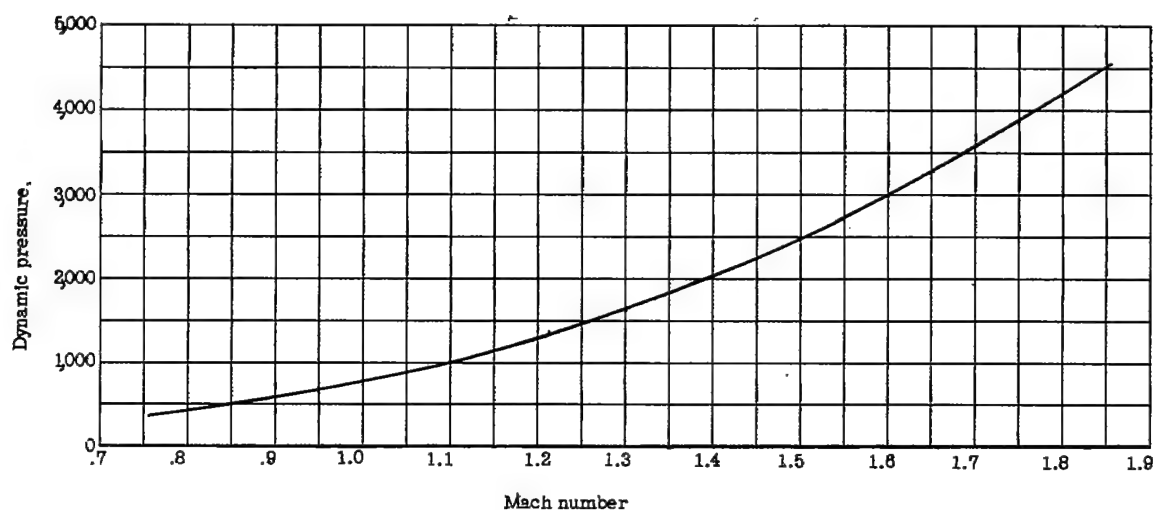


Figure 4.- Variation of dynamic pressure with Mach number.

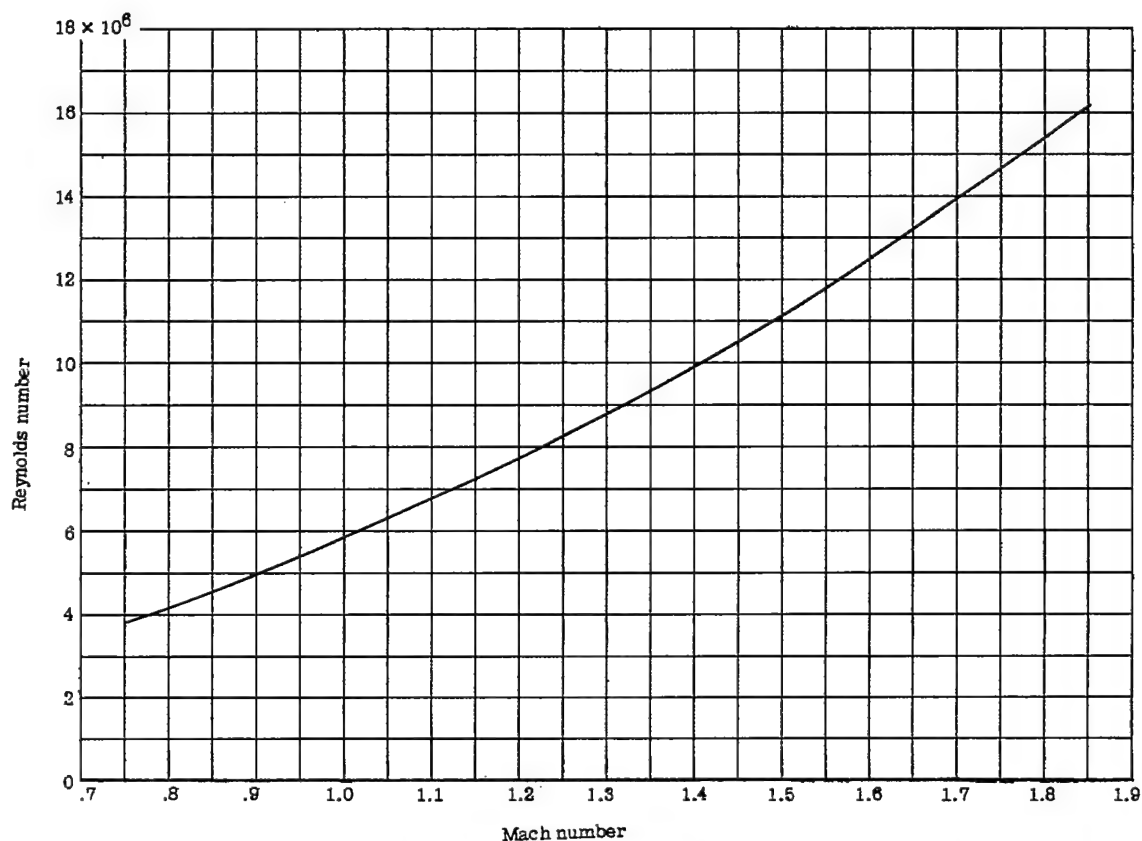


Figure 5.- Variation of Reynolds number with Mach number.

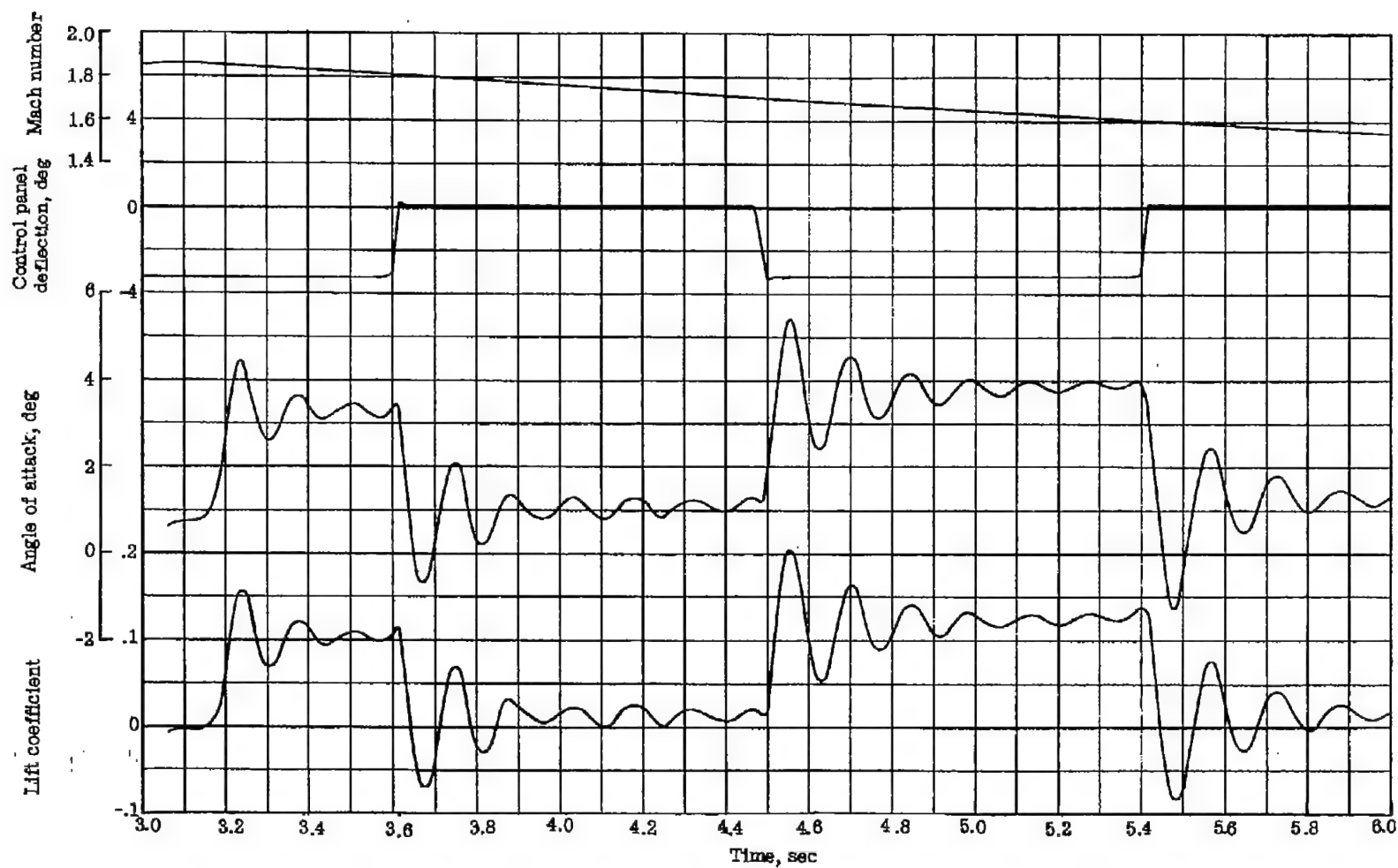
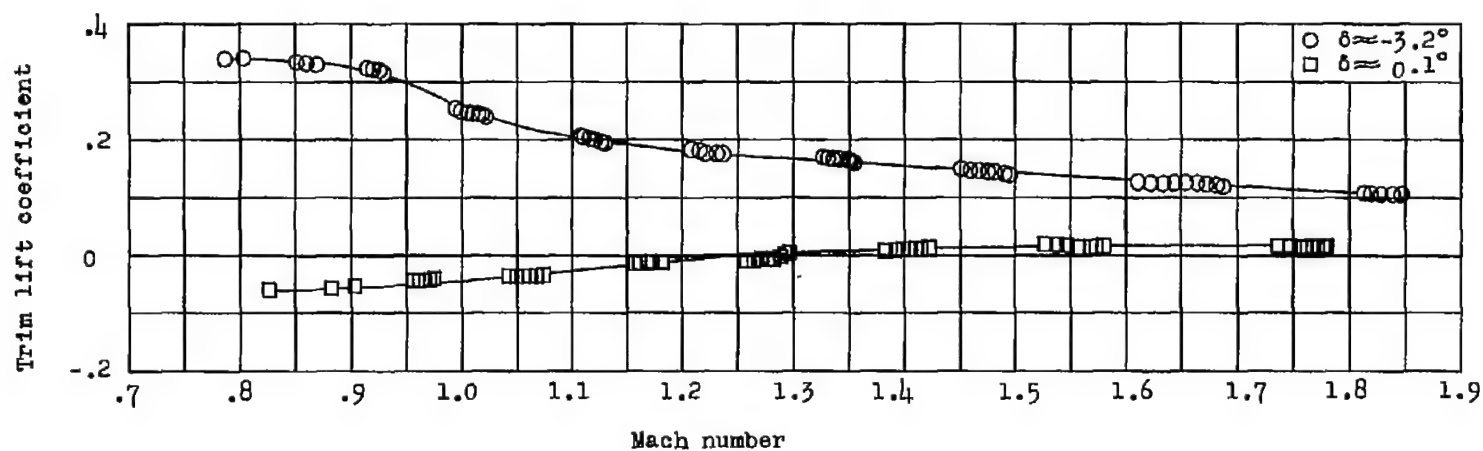
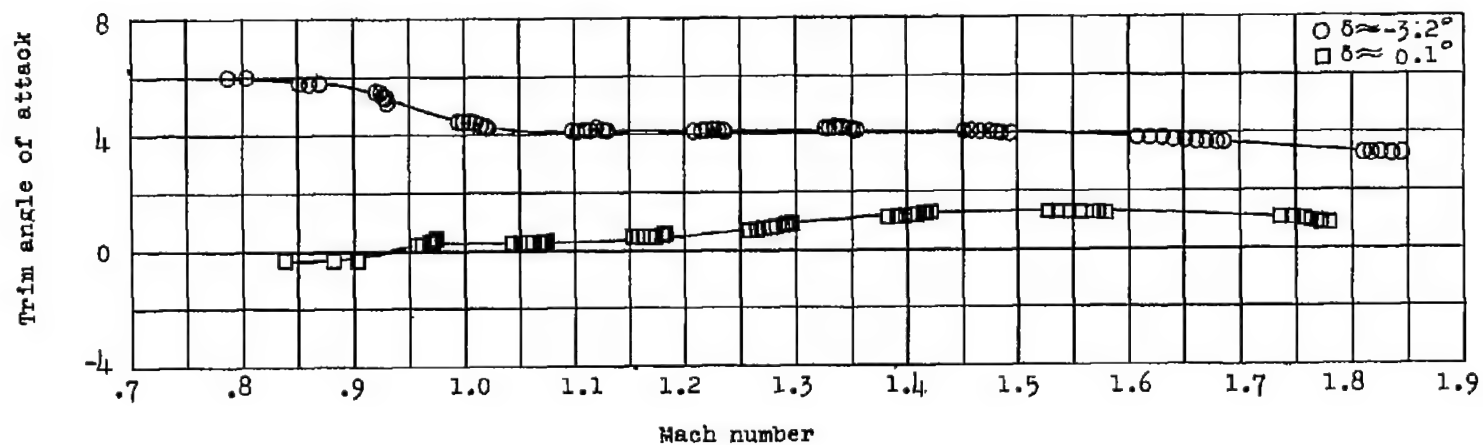


Figure 6.- Time history during first portion of flight of some quantities obtained in present investigation.

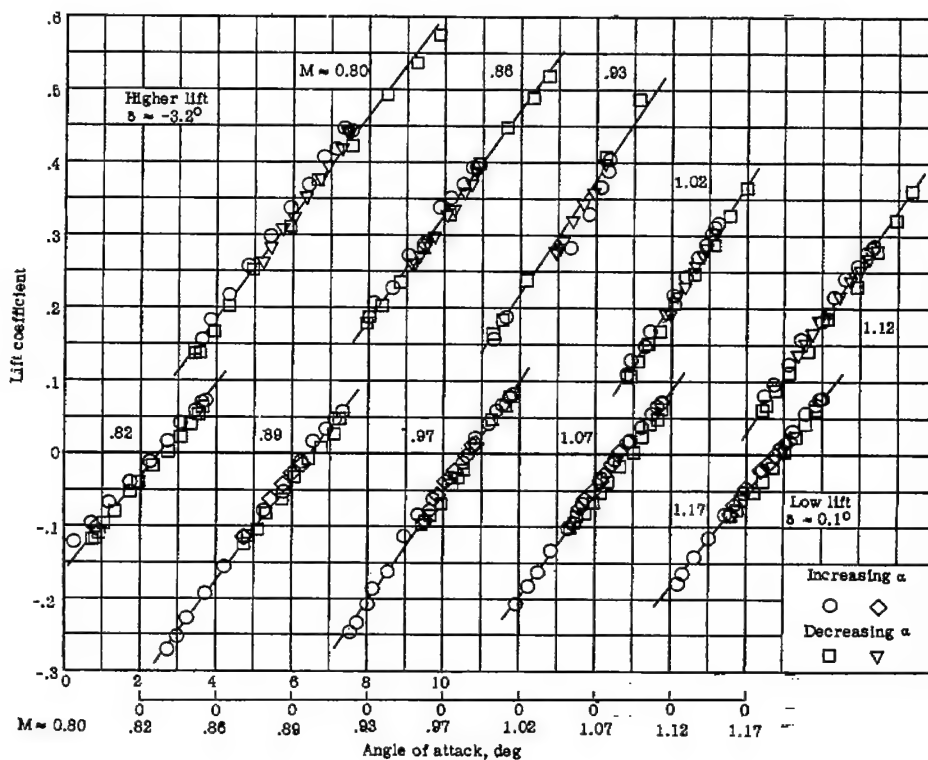


(a) Trim lift coefficient.

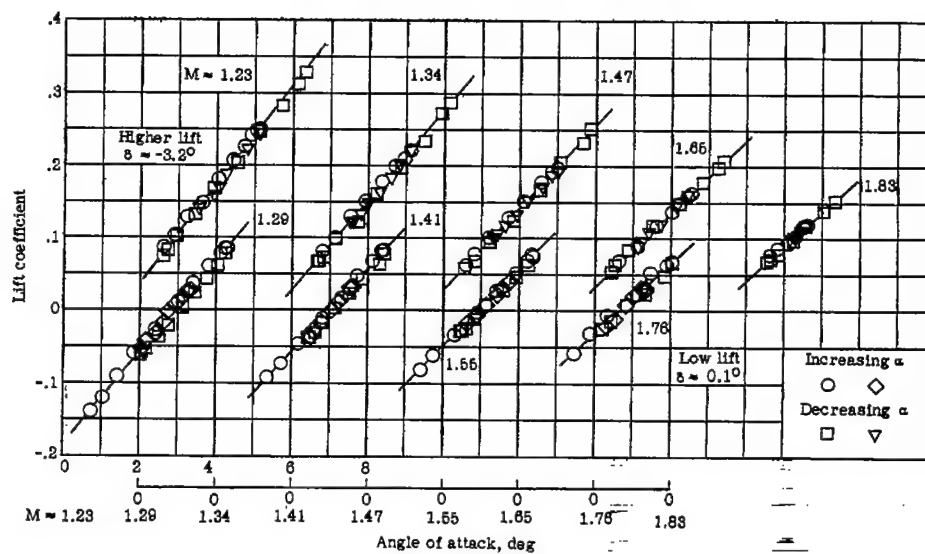


(b) Trim angle of attack.

Figure 7.- Longitudinal trim characteristics as a function of Mach number.



(a) Transonic Mach numbers.



(b) Supersonic Mach numbers.

Figure 8.- Variation of lift coefficient with angle of attack at transonic and supersonic Mach numbers.

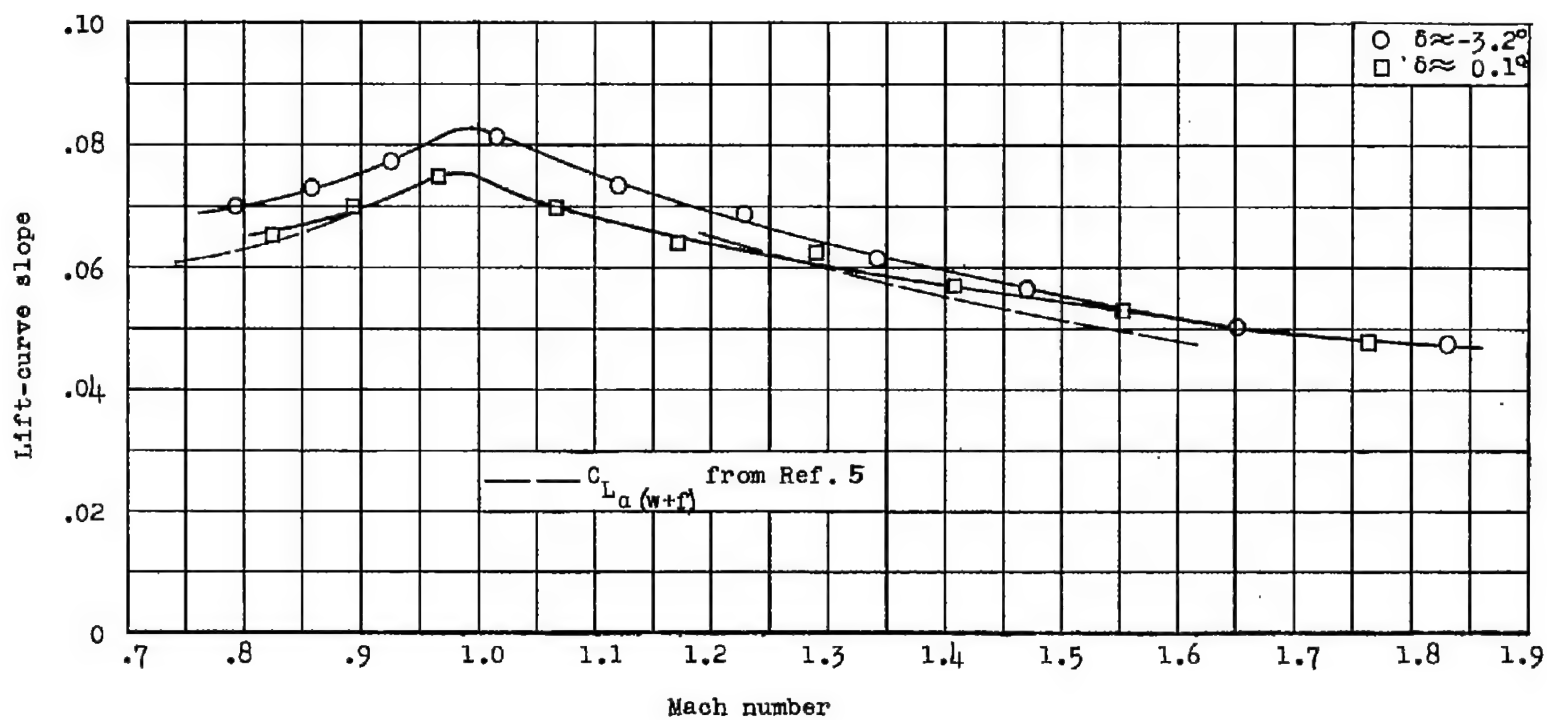


Figure 9.- Variation of lift-curve slope with Mach number.

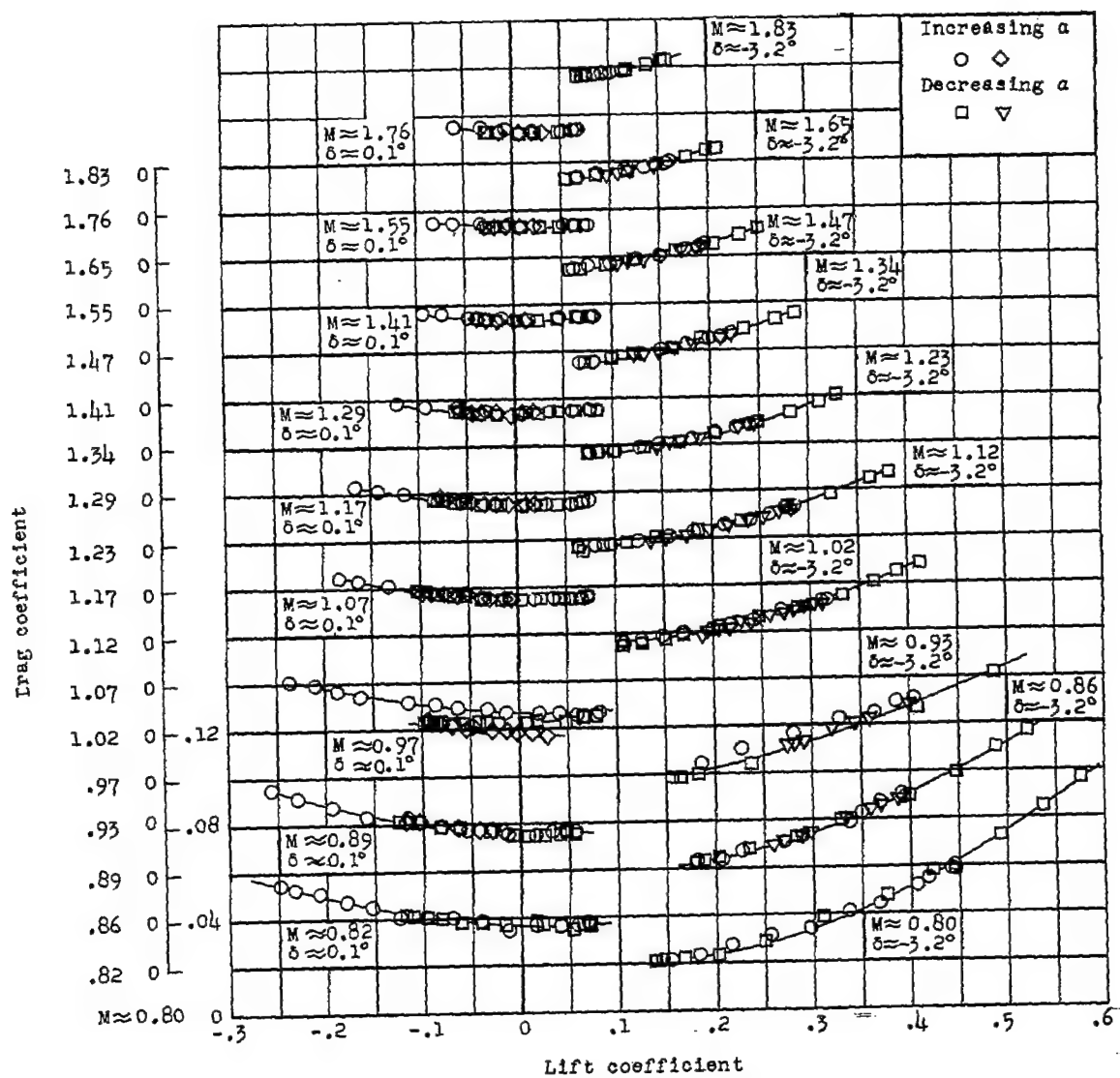
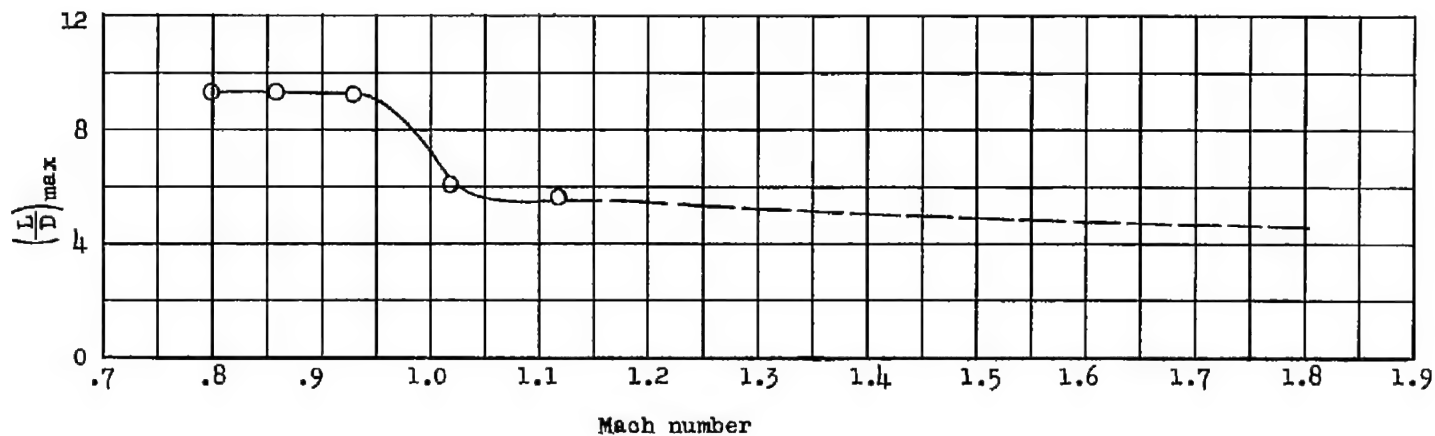
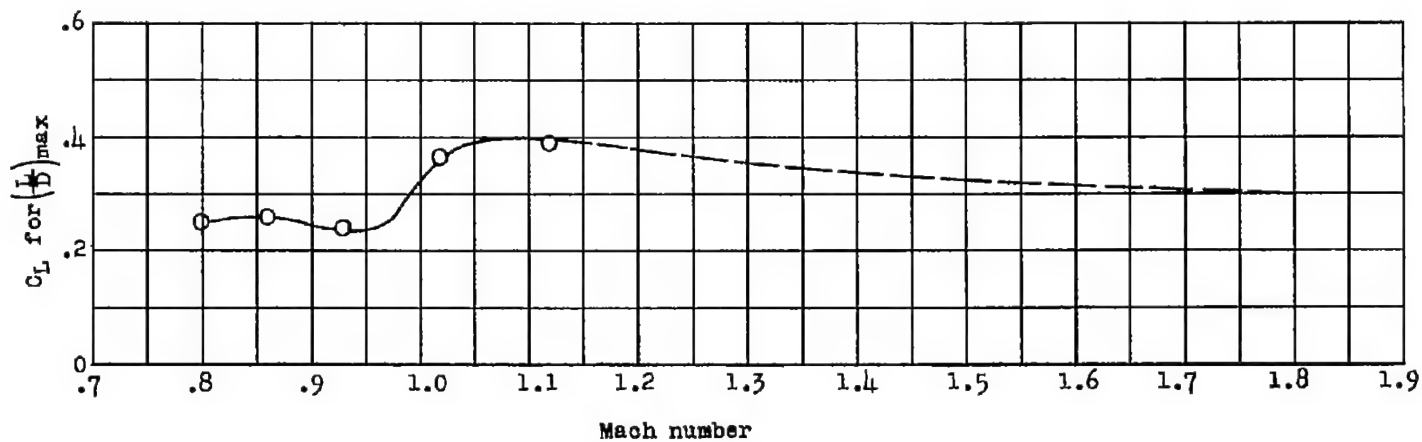


Figure 10.- Variation of drag with lift.



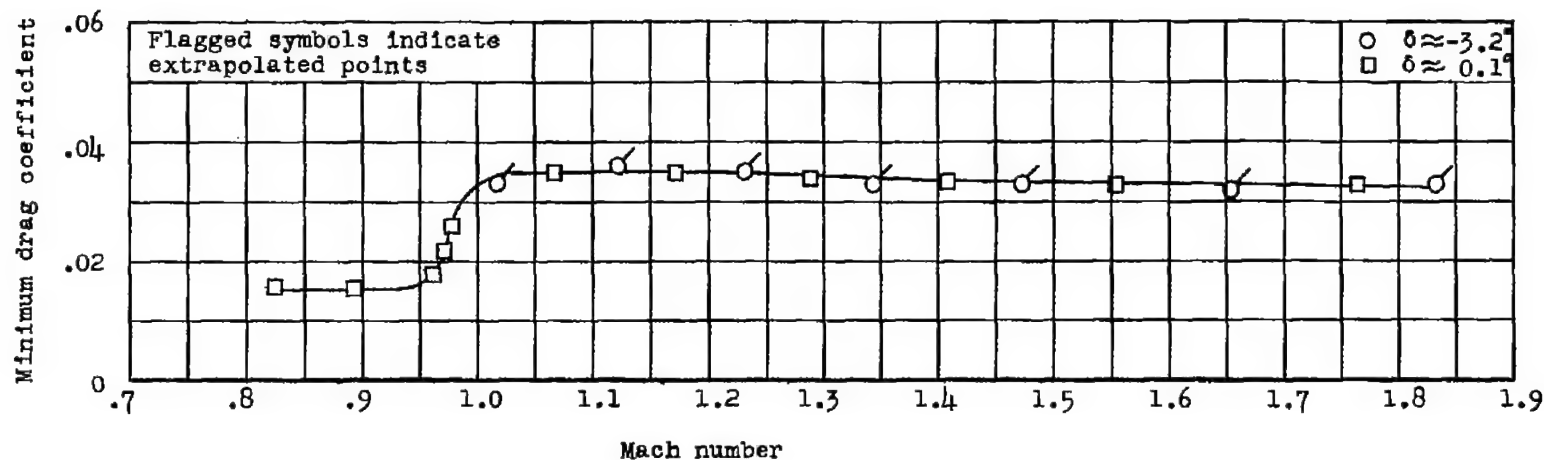


(a) Maximum lift-drag ratios.

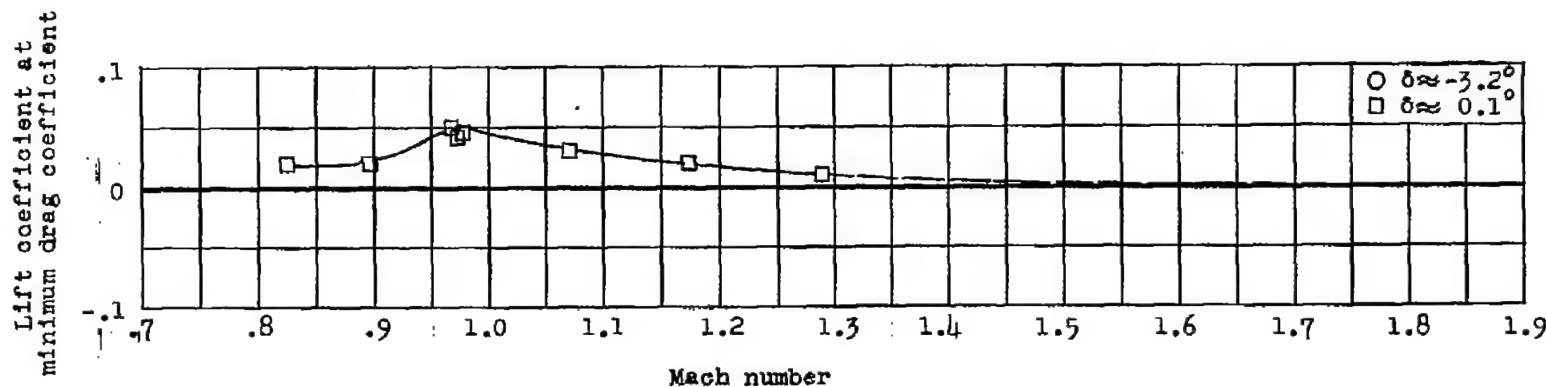


(b) Lift coefficients at which maximum lift-drag ratios occur.

Figure 11.- Variation of maximum lift-drag ratios and lift coefficients at which maximum lift-drag ratios occur as a function of Mach number.



(a) Minimum drag coefficient.



(b) Lift coefficient at minimum drag coefficient.

Figure 12.- Variation of minimum drag coefficient and lift coefficient at minimum drag coefficient as a function of Mach number.

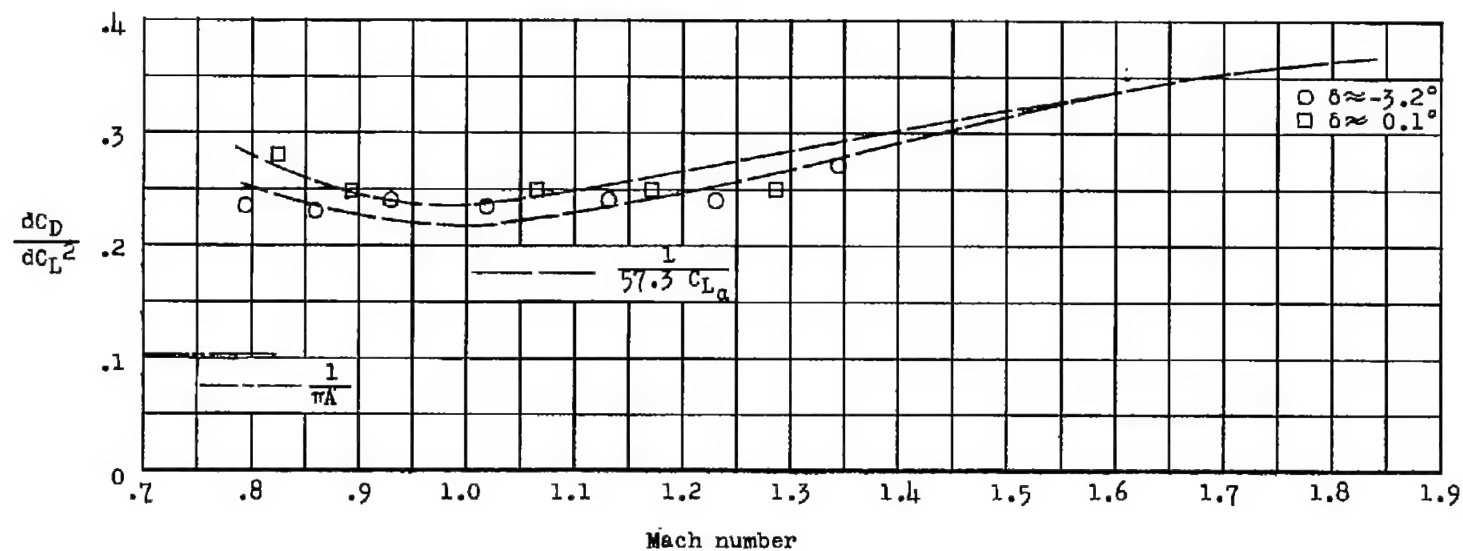


Figure 13.- Effect of lift on drag as a function of Mach number.

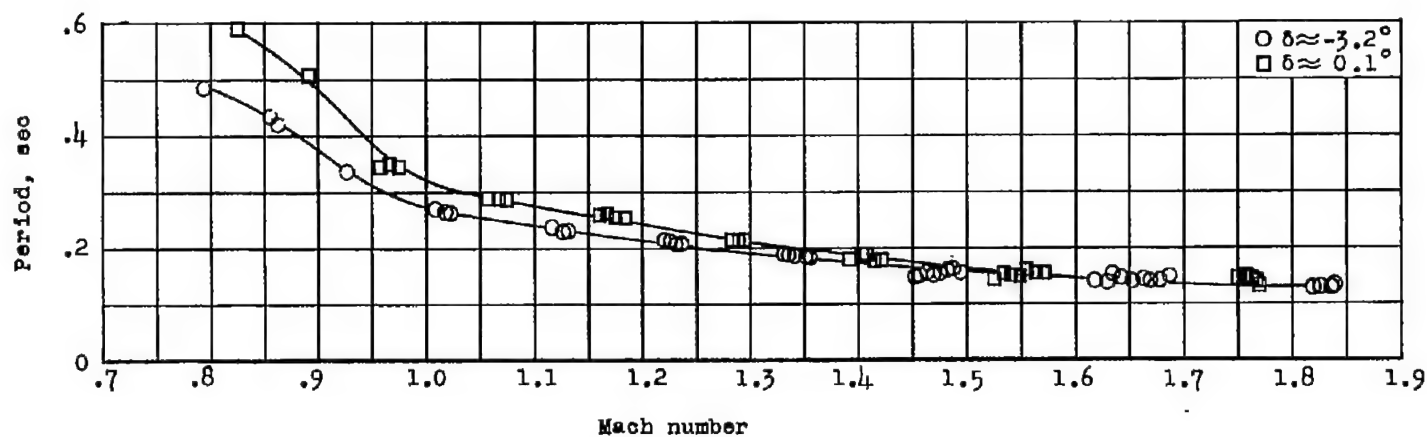


Figure 14.- Variation of measured period with Mach number.

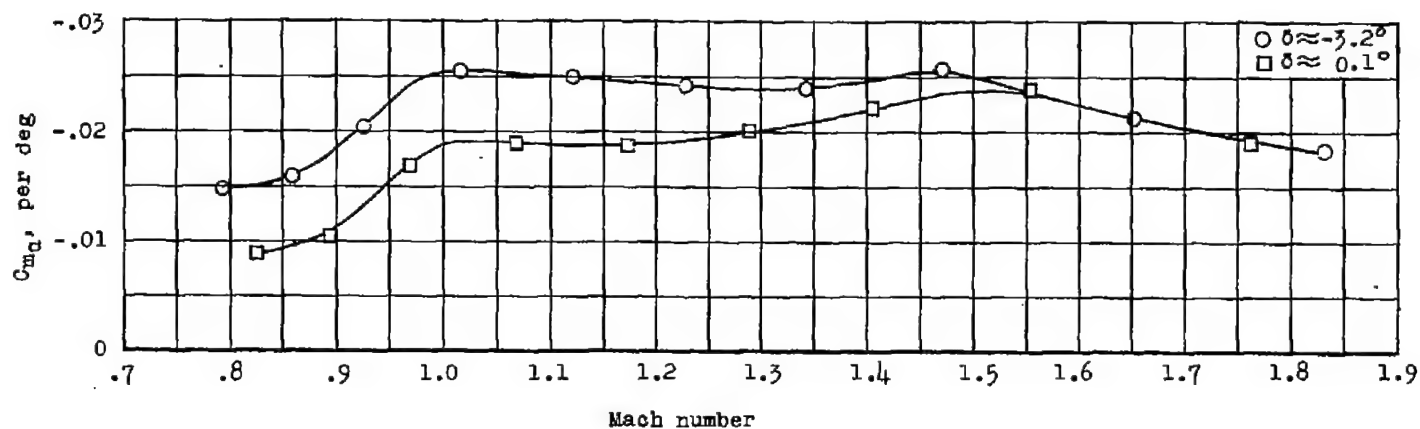


Figure 15.- Variation of static-stability parameter with Mach number.

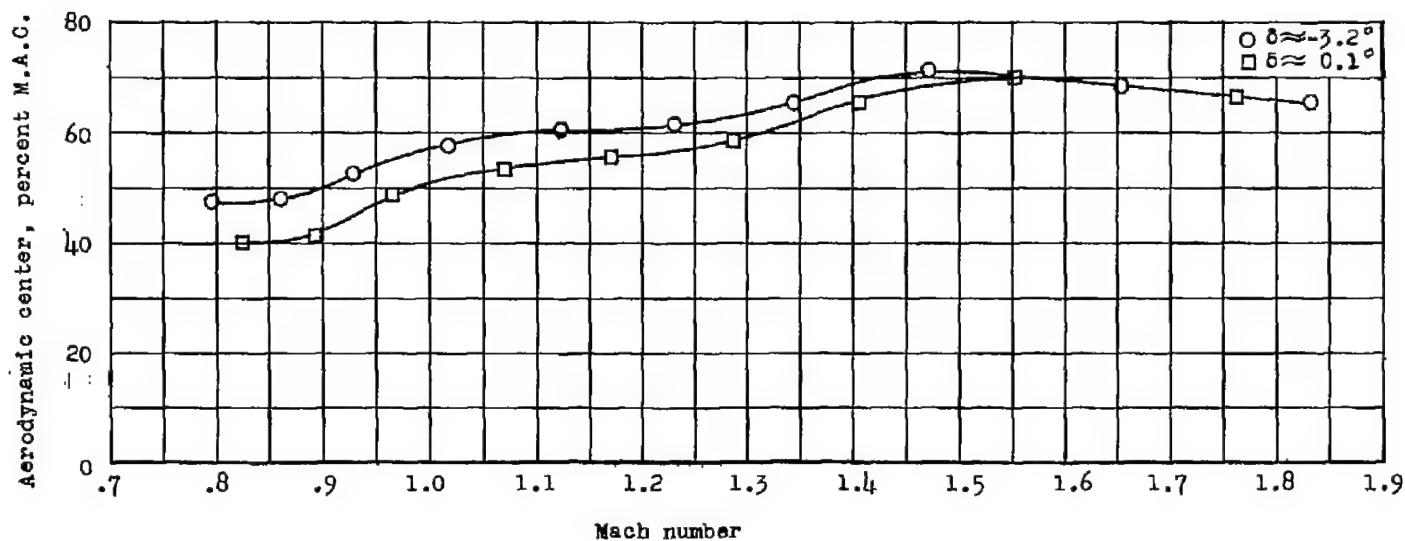


Figure 16.- Variation of aerodynamic center with Mach number.

CONFIDENTIAL

CONFIDENTIAL

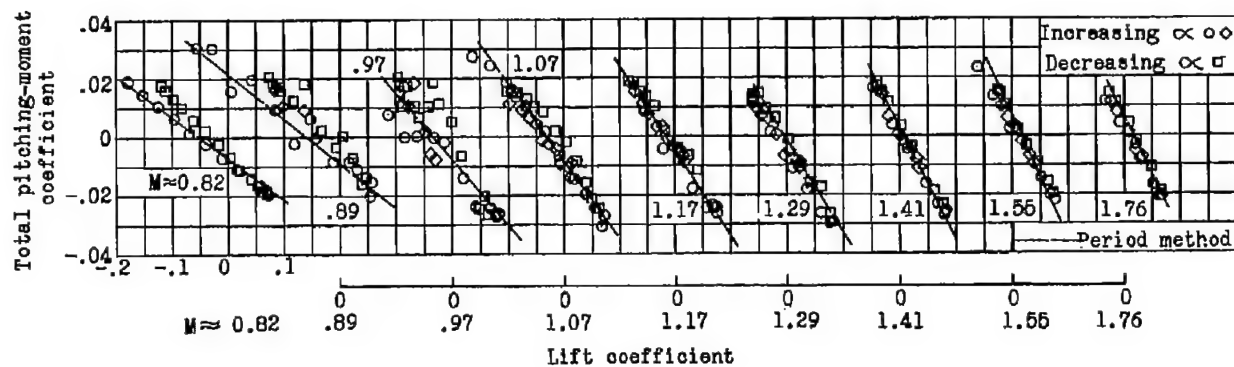
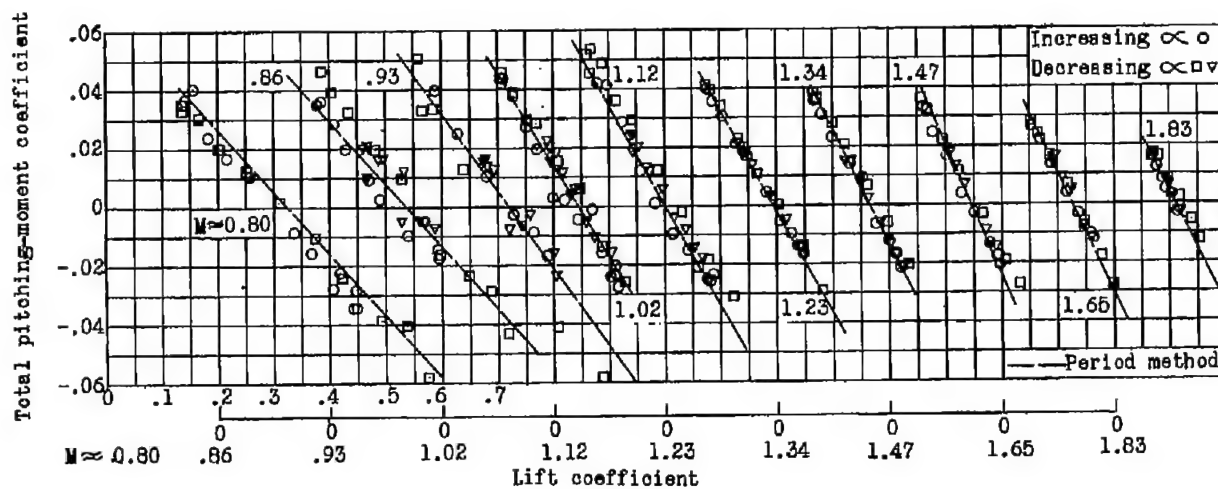
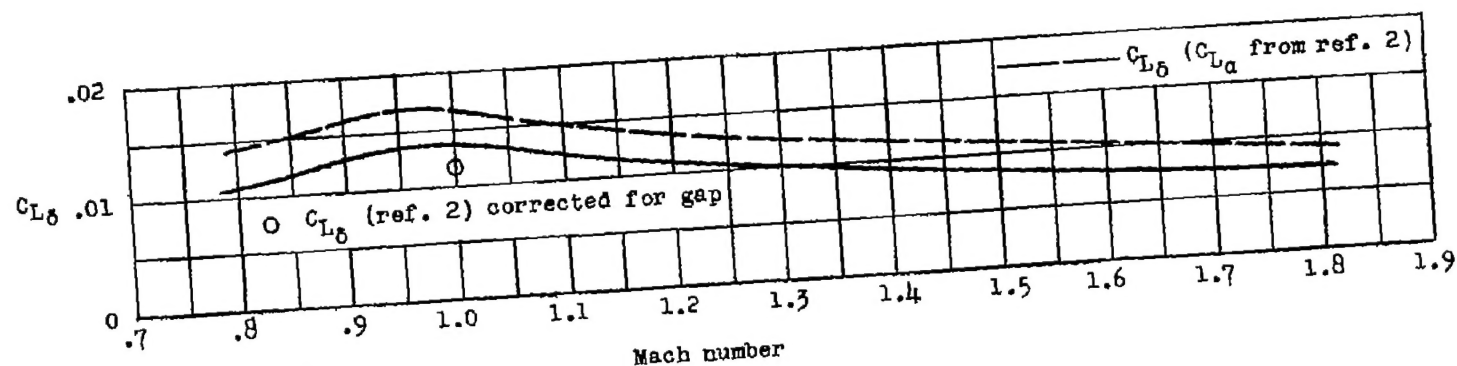
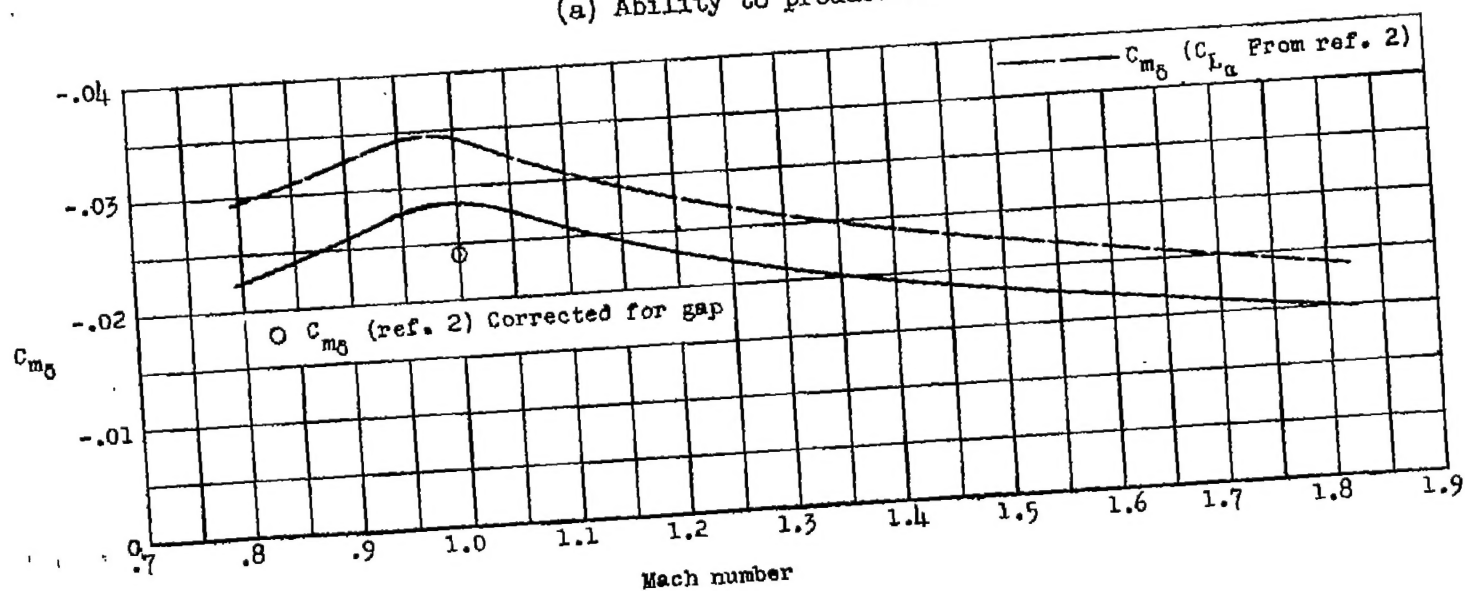
(a)  $\delta \approx 0.10^\circ$ .(b)  $\delta \approx -3.2^\circ$ .

Figure 17.- Variation of total pitching-moment coefficient with lift coefficient.



(a) Ability to produce lift.



(b) Effectiveness in producing moment.

Figure 18.- Variation of ability of horizontal tail to produce lift and effectiveness in producing moment as a function of Mach number.

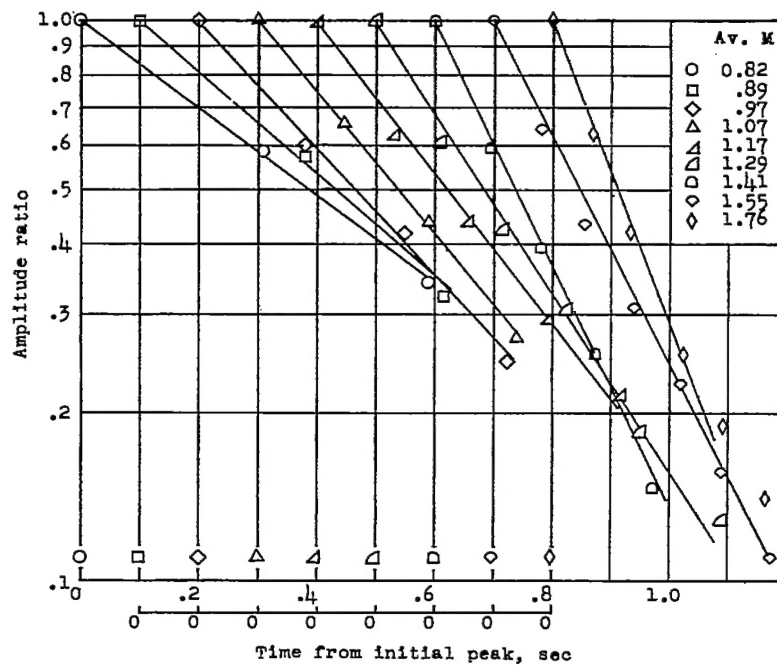
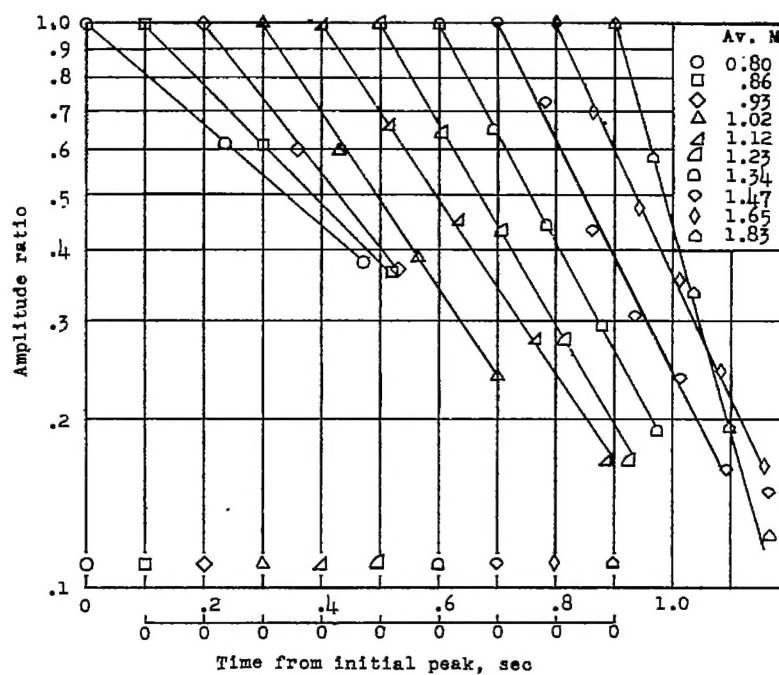
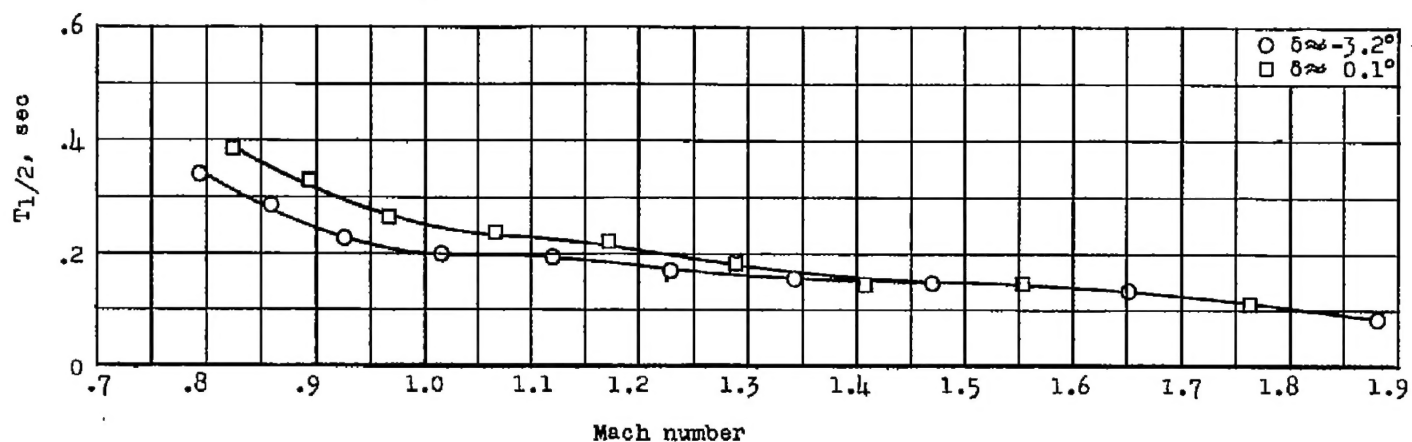
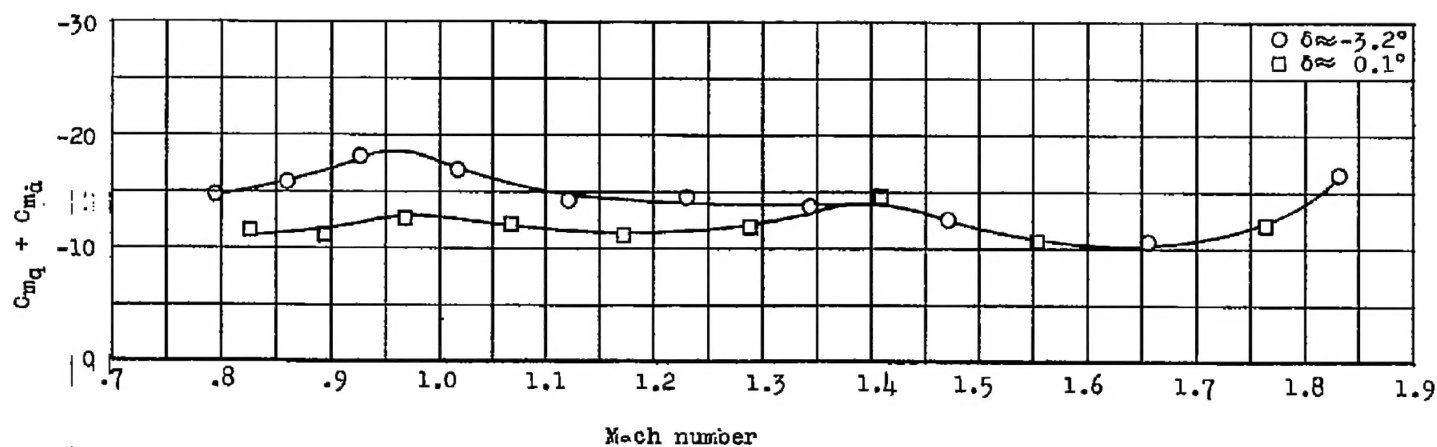


Figure 19.- Variation of amplitude ratio with time.



(a) Time to damp to one-half amplitude.



(b) Pitch damping-moment factor.

Figure 20.- Variation of damping characteristics of short period oscillations with Mach number.



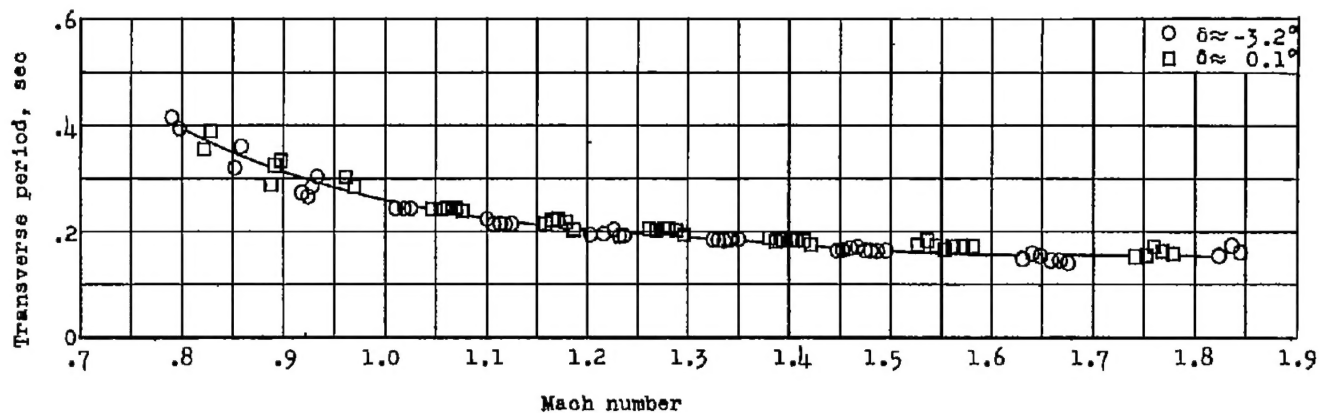


Figure 21.- Variation of measured period of lateral oscillation with Mach number.

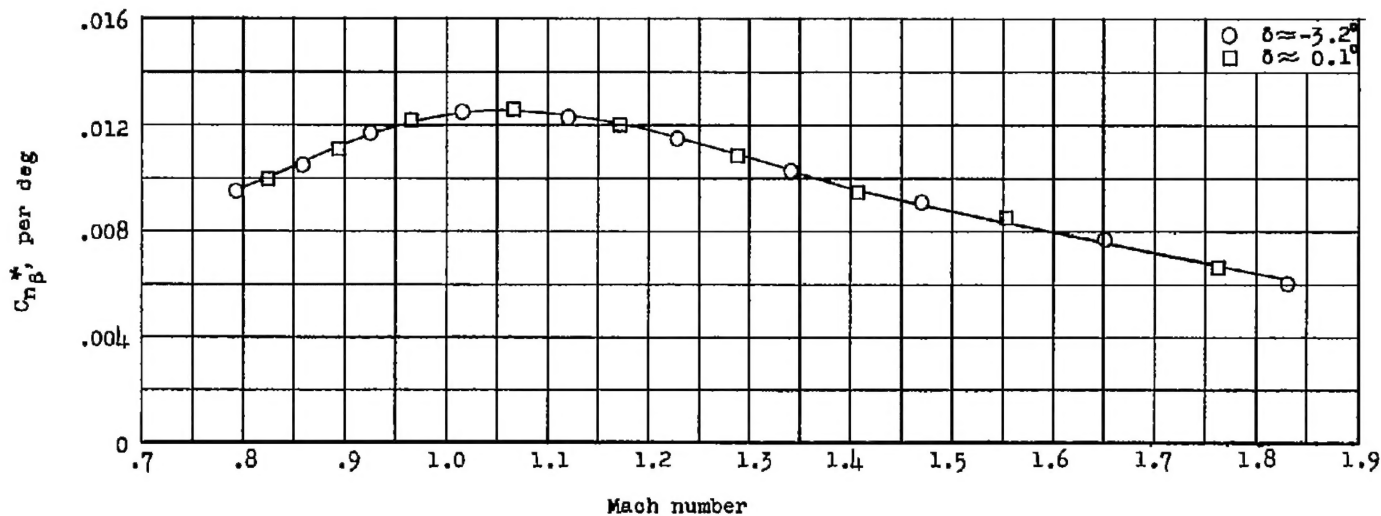


Figure 22.- Variation of static-directional-stability coefficient with Mach number.